Preprints (www.preprints.org) | NOT PEER-REVIEWED | Posted: 6 July 2021 doi:10.20944/preprints202107.0155.v1

Long-range static and dynamic previtreous effects in supercooled squalene - impact of strong electric field

Szymon Starzonek*, Aleksandra Drozd-Rzoska, Sylwester J. Rzoska,
Institute of High Pressure Physics of the Polish Academy of Sciences, 29/37 Sokołowska Str. 01-142 Warsaw, Poland
*Corresponding author's email: starzoneks@unipress.waw.pl

ABSTRACT

The evidence is presented for the long-range previtreous changes of two static properties: dielectric constant (ε) and its strong electric field related counterpart - the nonlinear dielectric effect (NDE). Notable is the evidence for the functional characterizations of $\varepsilon(T)$ temperature changes by the 'Mossotti Catastrophe' formula, and NDE vs. T evolution by the relations resembling one developed for critical liquids. The analysis of dynamic properties based on the activation energy index excluded the Vogel-Fulcher-Tammann (VFT) relation as a validated tool for portraying the evolution of the primary relaxation time. Such a result questions the commonly applied 'Stickel operator' routine as the reliable tool for determining the dynamic crossover temperature. It is worth stressing that the strong electric field radically affects the distribution of relaxation times, the form of the evolution of the primary relaxation time as well as the fragility. Obtained results support the concept of a possible semi-continuous phase transition hidden below T_g. Studies were carried out in supercooled squalene, the material with extremely low electric conductivity, strongly elongated molecule, and vitally important for biology and medicine related issues.

Keywords: molecular liquid; nonlinear dielectric effect; glass transition; ODIC; pretransitional effect

I. INTRODUCTION

The problem of supercooled liquids has remained an intensive field of research for decades. Notwithstanding, it is still located amongst fundamental grand challenges for the 21st-century science. One of the hallmark features that particularly attract attention is long-range previtreous changes of dynamic properties, starting even 100 K above the glass temperature T_g , for viscosity η or equivalently the primary relaxation time τ. There is a widespread belief that previtreous effects are only related to dynamic properties, exhibiting some hallmarks of universality, conceptually expressed by the Super-Arrhenius (SA) relation:

$$\tau(T) = \tau_0 \, exp\left(\frac{E_a(T)}{RT}\right) \qquad (1)$$

where $E_a(T)$ denotes the apparent, temperature-dependent activation energy. Parallel relations take place for $\eta(T)$ or $\sigma(T)$ behaviour. It is empirically stated that glass temperature T_g may be defined as a temperature when $\tau(T) \approx 100s$ and $\eta(T) \approx 10^{13} Poise$. For low-molecular-weight-liquid, the pre-exponential factor $\tau_0 \sim 10^{-14} s$. For the basic Arrhenius dependence Arrhenius dependence $E_a(T) = E_a = const$, in the given temperature domain.

There are some indications for previtreous changes for the heat capacity, the most representative thermodynamic magnitude. However, they appear only in a narrow range of temperatures above T_g and no common functional description has been found so far.

This report presents the evidence for long-range previtreous changes of dielectric constant, the basic 'static' property. They are associated with specific previtreous evolution of

Preprints (www.preprints.org) | NOT PEER-REVIEWED | Posted: 6 July 2021 doi:10.20944/preprints202107.0155.v1

dynamic properties. Also, these extends to the behaviour under the strong electric field, tested in a way hardly explored so far

The mentioned behaviour has been found in squalene, $(C_5H_8)_6$, triterpene), the compound with enormous biological [1], medical potential [2, 3] and hence used in the pharmaceutical [4, 5] and food [6, 7] industries. Due to its emollient, skin hydration, antioxidant and anticancer properties. The dietary presence of squalene in olive oil was suggested as the key factor reducing cancer mortality in Mediterranean countries [7]. However, its synthesis and characterization still constitute a challenge for chemists and biochemists [8-10]. From this point of view, squalene, namely 2,6,10,15,19,23-hexamethyl-2,6,10,14,18,22-tetracosahexaene, is a naturally occurring terpenoid hydrocarbon, with a strongly elongated form and a weak permanent dipole moment ($\mu \approx 0.6D$) [11]. The important feature of squalene is the extremely low electric conductivity what essentially facilitates measurements under the strong electric field, enabling the minimization of biasing effect impacts of electric conductivity.

When discussing the previtreous dynamics, it is notable that the SA Eq. (1) has mainly the cognitive meaning and cannot be used for portraying experimental data due to the unknown form of the apparent activation energy. Consequently, replacement scaling relation has to be developed. For decades the leading position occupied the Vogel-Fulcher-Tamman (VFT) relation:

$$\tau(T) = \tau_0 \, exp\left(\frac{D_T T_0}{T - T_0}\right) \tag{2}$$

where T_0 is the VFT estimation of the ideal glass temperature, also linked to a hypothetical phase transition; D_T is the fragility strength coefficient.

Comparing Eqs. (1) and (2) one obtains: $E_a(T) = RDT_0/t$, where $t = (T - T_0)/T$ is the relative dimensionless distance from the singular temperature T_0 . Worth recalling is the link of the SA Eq. (1) to the fragility, the basic 'quasi-universal metric for the previtreous behavior, showing the distrortion from the reference Arrhenius behavior:

$$m = \left[\frac{d\, log_{10}\, \tau(T)}{d(T_g/T)}\right]_{T=T_g} \tag{3}$$

For the basic Arrhenius behaviour $m = log_{10}\, \tau(T_g) - log_{10}\, \tau_0 \approx 16$. The weak slowing down below the Arrhenius pattern is related to $m < 30$ and referred to as the 'strong' glass former. Systems with the essential SA dynamics, and $m > 30$ are called 'fragile'. The maximal reported value: $m > 200$ [15]. One can extend Eq. (3) into the previtreous domain introducing $m(T > T_g)$ as the apparent fragility, also known as the steepness index. Comparing Eqs. (1)-(3) one obtains: $D_T = 590/(m - 16)$. The enormous previtreous slowing down indicates the broadband dielectric spectroscopy (BDS) as the key research tool since it can cover 12-17] decades in frequency/time during a single measurement process. It can detect the primary relaxation time, including the distribution, other relaxation processes, DC electric conductivity, etc.

In the last decade, the omnipotence and fundamental importance of the VFT relation have been fundamentally questioned. It led to the emergence of competing dependences. Worth recalling here is the MYEGA equation, avoiding the final temperature singularity [21]:

$$\tau(T) = \tau_0 \, exp\left(\frac{K}{T} exp\left(\frac{C}{T}\right)\right) \tag{4}$$

where $T > T_g$, K and C are constants.

For liquid-crystalline and plastic crystal glass formers, the prevalence of the critical like description was shown [22-26]:

Preprints (www.preprints.org) | NOT PEER-REVIEWED | Posted: 6 July 2021 doi:10.20944/preprints202107.0155.v1

$$\tau(T) = \tau_0 (T - T_C)^{-\phi} \quad (5)$$

where $T > T_g$ and $T_C < T_g$; the power exponent $8.5 < \phi < 15$.

Such basic properties as dielectric constant, primary relaxation time, or electric conductivity are precisely determined from broadband dielectric spectroscopy (BDS) scans. The maturity of BDS method applied for glass-forming systems poses the question of its successor. The natural candidate is the Nonlinear Dielectric Spectroscopy (NDS), the strong electric field related to BDS [29-37]. Considering polarizability as the function of the intensity of the electric field one obtains [37]:

$$P(E) = \chi^* E + \Delta\chi^* E^3 + \ldots \quad (6)$$

where $\chi^* = \varepsilon^* - 1$ is for the complex dielectric susceptibility and ε^* is for dielectric permittivity.

It is well known that BDS is directly coupled to 2-point correlation function, whereas NDS to 4-point one. This fact shows that NDS-based study can radically deepen the insight into the still mystic nature of the previtreous state. The progress in NDS studies of glass formers has led mainly to developing the phenomenological description of 'nonlinear' spectra in various materials. However, no temperature dependence for the previtreous behaviour under the strong electric field has been postulated so far [29-34].

It is worth recalling here that studies of pretransitional phenomena appeared to be the key for the grand success of the Physics of Critical Phenomena [38-40]. However, there are striking differences between precritical and previtreous phenomena, namely: (i) precritical phenomena are associated with a well-defined phase transition, (ii) practical changes are observed for dynamic, static, and thermodynamic physical properties, (iii) the universality is associated not only with the form but also values of universal parameters (critical exponents, ratios of critical amplitudes) [38-40]. These basic features seem to be absent or at least disputable for the glass transition and previtreous effects [12-17, 27-37].

This article shows the evidence for long-range previtreous behaviour of the dielectric constant and its strong electric field related counterpart - the nonlinear dielectric effect, *NDE* in supercooled squalene. That dielectric constant follows the 'Mossotti Catastrophe' functional pattern, so far considered as the 'forbidden state' in dipolar liquids. This result is supplemented by analysing the primary relaxation time evolution under weak and strong electric field. The application of the distortions-sensitive analysis revealed features of the previtreous dynamics. Such a way of analysis minimizes the key problem of data analysis in the previtreous region, associated with the fact that it is located well above the hypothetical, hidden, singular temperature.

II. EXPERIMENTAL

In our studies, we used the broadband dielectric spectrometer (BDS, Novocontrol), supported by the strong electric field facility enabling nonlinear dielectric spectroscopy studies and the Quattro temperature control unit with the temperature stability better than ΔT=0.02 K [42]. Samples were placed in a flat-parallel gold-coated measurement capacitor with plates made from Invar: diameter $2r = 20$ mm and the gap $d = 0.15$ mm. Quartz ring was used as the spacer. Scans of dielectric properties were carried out in the frequency range $0.1\ \text{Hz} < f < 10\ \text{MHz}$ under the weak measuring voltage $U_{weak} = 3$ V, corresponding to the electric field $E_{weak} = 0.2\ kV/cm$. The scan of dielectric properties under the strong electric field was carried out for U_{strong}~1000 V. i.e., for $E_{strong} = 60 - 70\ kV/cm$, and $f < 10$ kHz - using the High Voltage Novocontrol facility [42, 43].

To the best of the authors' knowledge, the nonlinear dielectric studies in glass-forming systems are focused mainly on dynamics issues and still have not to lead to conclusive temperature

Preprints (www.preprints.org) | NOT PEER-REVIEWED | Posted: 6 July 2021 doi:10.20944/preprints202107.0155.v1

dependences of tested properties, including the functional description. This report concentrates on the static part of NDS, the nonlinear dielectric effect (NDE) [43-45], hardly tested for glass-forming systems so far $\varepsilon(E)=\varepsilon(E\to 0)+\Delta\varepsilon E^2+\ldots$, where $\varepsilon(E\to 0)=\varepsilon$ represents the dielectric constant and then:

$$NDE := \frac{\Delta\varepsilon}{E^2}=\frac{\varepsilon(E)-\varepsilon}{E^2}=\frac{\Delta\chi}{E^2} \quad (7)$$

where χ denotes the dielectric susceptibility: $\chi=\varepsilon-1$.

The notable features for measurement under the strong electric field are the bulk gap of the measurement capacitor and degassing of samples immediately prior to the experiment. These essentially reduce the risk of gas bubbles in the sample, which can qualitatively distort measurement results under the strong electric field. Notable was extremely low electric conductivity, which causes no heating of sample during measurements under the strong electric field, well-evidenced basing factor in such studies. Finally, the occurrence of the condition $NDE\propto E^2$ has been carefully tested. The key target of dielectric studies under the strong electric field were find temperature changes of tested properties, possible for functional evaluations.

III. RESULTS and DISCUSSION

This paper is focused on the behaviour under strong and weak electric fields, including dynamic and static issues related to dielectric studies. However, before the basic reference, BDS related behaviour in supercooled squalene is presented. Figure 1a shows selected spectra for the imaginary part of dielectric permittivity in supercooled squalene in the vicinity of the glass temperature. Peaks of main loss curves determine primary relaxation times $\tau=1/\omega_{peak}=1/2\pi f_{peak}$ [15, 27]. In the immediate vicinity of the glass temperature, estimated via the empirical condition $\tau(T_g)\approx 100s$ as $T_g\approx 164K$ the secondary fast relaxation (beta) process emerges. For slightly higher temperatures, the low-frequency relaxation (LF) process, disappearing on $T\to T_g$ was observed. Temperature evolutions of basic relaxation processes resulting from the analysis of dielectric spectra are shown in Fig. 1b. The primary relaxation time shows clear SA behaviour (Eq. (1)). Its optimal portrayal is described further in the report. Well below T_g the low-frequency process (LF) also occurs, and in the immediate vicinity of T_g the secondary (beta) process emerges and smoothly continues deeper into the solid glass state, for $T<T_g$.

Preprints (www.preprints.org) | NOT PEER-REVIEWED | Posted: 6 July 2021 doi:10.20944/preprints202107.0155.v1

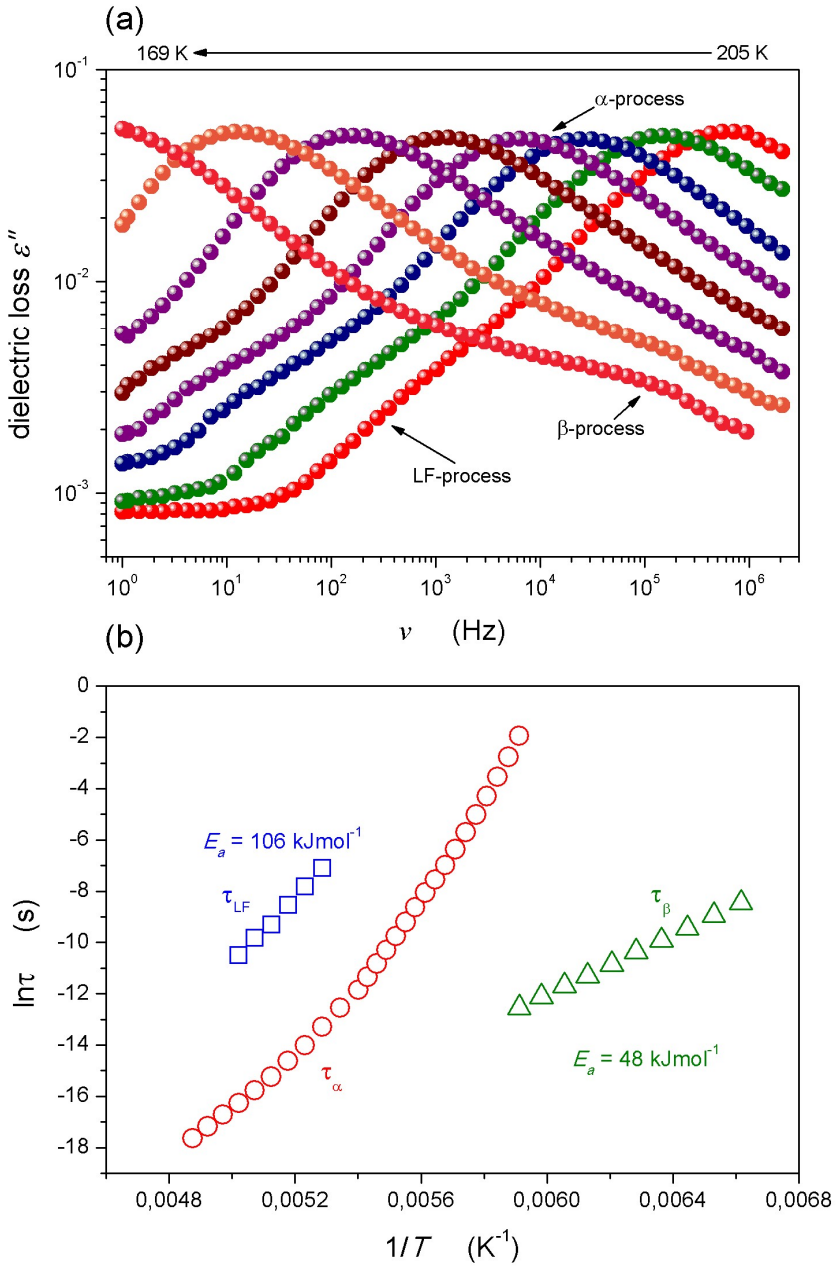

Figure 1 (a) Broadband dielectric loss spectra for supercooled squalene at temperatures 201 – 169 K. **(b)** distribution of relaxation times: Arrhenius behaviour for low-frequency and secondary processes, VFT behaviour for primary relaxation. The activation energies were calculated via Arrhenius equation $\tau(T) = \tau_0 \exp(-E_a/RT)$. For obtaining β-process the temperature range 201-151 K was used.

Stevenson and Wolyness [46] suggested universal origins of the beta process showing that by adding fluctuations to the existing structure of the random first-order transition theory, a tail develops on the low free energy side of the activation barrier distribution, which shares many of the observed features of the secondary relaxations Consequently they suggested that while primary relaxation takes place through activated events involving compact regions, secondary relaxation is governed by more ramified, string-like, or percolation-like clusters of particles. When considering Fig.1b one can conclude that such a mechanism has to be valid

Preprints (www.preprints.org) | NOT PEER-REVIEWED | Posted: 6 July 2021 doi:10.20944/preprints202107.0155.v1

also in the solid glass states below T_g where bonds stabilizing the liquid-like arrangement in amorphous solid form develops.

The analysis of the SA temperature evolution for the primary relaxation time most often involves its portrayal by the selected model dependence (for instance Eq. (3-5) by the determination of the fragility (Eq. (2)) and the search for the dynamical crossover phenomenon via the so-called Stickel analysis based on the plot $\left[d\ln\tau(T)/d(1/T)\right]^{-1/2}$ vs. $1/T$ [15, 47]. In this work, we avoid the latter because it is assumed a priori that the VFT Eq. (3) obeys [48, 49]. Prior to fitting experimental data by an arbitrarily selected model-relation, the optimal model equation was found. Finally, instead of focusing on the value of the fragility at T_g (Eq. (2) the analysis of the apparent fragility and the activation energy for the whole previtreous domain was performed. These procedures are implemented below, and the behaviour both under weak and strong electric field is discussed.

The survey of available results concerning the previtreous domain revealed a surprising gap regarding the temperature behaviour of such basic property as the dielectric constant [12-17, 21-37 and refs. therein]. Our results for squalene eliminate this gas - see Fig. 2. It is worth noting that the presented value is always related to the midpoint of the static domain and considers its strong shift towards lower frequencies on cooling towards T_g. Lack of DC conductivity impacts in the case of squalene. The scale applied in Figure 1 reveals the temperature behaviour described in the broad temperature range also affects the obtained results by the relation:

$$1/\varepsilon = a + bT \qquad \chi = \varepsilon - 1 = \frac{1}{a+bT} = \frac{1/b}{T - a/b} = \frac{A}{T - T^{+}} \tag{8}$$

and then $T^{+} = a/b$ and $A = 1/b$.

For the high-temperature domain $T_B(?) < T < T_b$ one obtains $a = 0.142$ and $b = 2.23\times10^{-4}$ and for $T < T_B(?)$ $a = 0.18_1$ and $b = 4.43\times10^{-5}$.

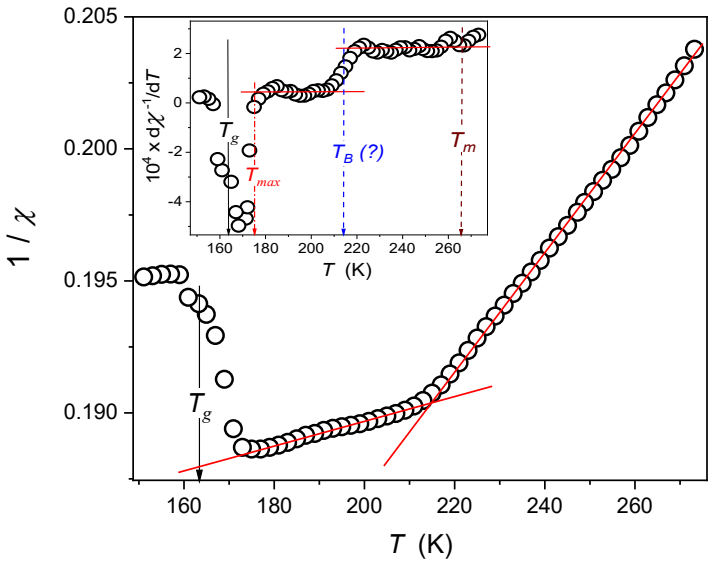

Figure 2 The temperature evolution of the reciprocal of dielectric constant in supercooling squalene. Red, solid lines are related to the description via Eq. (8). The inset is for the distortions-sensitive derivative of results from the central part of the plot. It additionally confirms the description via Eq. (8), by revealing some distortions close to T_g and strong changes near the hypothetical dynamic crossover temperature $T_B = 215K \pm 5$.

Preprints (www.preprints.org) | NOT PEER-REVIEWED | Posted: 6 July 2021 doi:10.20944/preprints202107.0155.v1

The distortions-sensitive plot in the inset to Figure 2 confirms the validity of Eq. (8), by additionally showing temperature T_B, for which the coincidence with the dynamic crossover temperature [15] can be considered.

Particularly notable is the correlation of Eq. (8) with the dependence known for so-called 'Mossotti Catastrophe' appearing when applying the Mossotti-Lorentz (ML) local field for dipolar liquids. Its occurrence is explained as the consequence of neglecting intermolecular interactions in the ML model. Its picturesque illustration is the 'impossible ferroelectricity' for water appearing at $T \sim 1100$ K. Figure 2 shows the evidence of such behaviour in supercooled squalene in the high temperature ($T > T_B$) and low temperature ($T < T_B$) dynamic domains. Only recently, a similar 'Mossotti Catastrophe' type behaviour was reported in liquid and orientational disordered crystal (ODIC) phaser of glass-forming cyclooctanol.

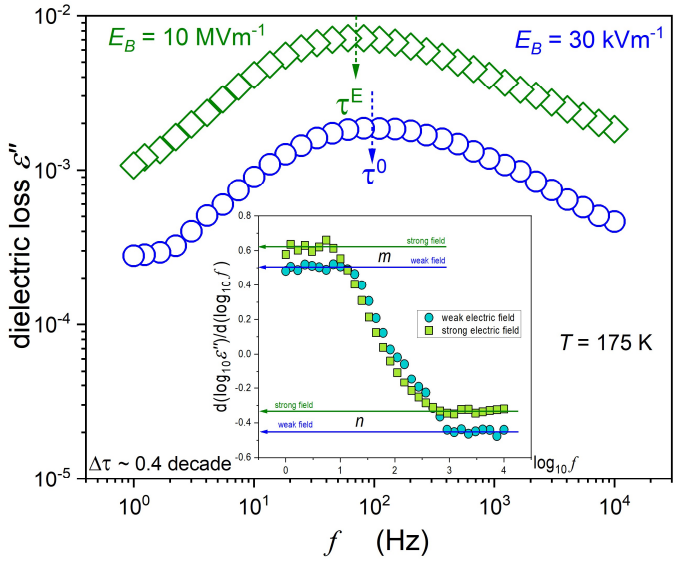

Figure 3 Dielectric loss spectra for low- and high-voltage applied to samples. The inset shows derivatives of experimental data from the main part of the plot and recalls the Jonsher's analysis via Eq. (10).

On of targets of presented studies was the behaviour of supercooled squalene under the strong electric field. Figure 3 focuses on dynamic issues, presenting the shift of primary loss curves under the strong electric field close to T_g. The obtained behaviour fairly coincides with one known from NDS studies reported so far. Notwithstanding, some features characteristic for the given system are worth stressing. The first one is the disappearance of the secondary relaxation process under the strong electric field. This means that structural relaxation-related differences between hypothetical multimolecular species/clusters/strings and their surroundings disappear under the strong electric field. The second feature is related to the inset which reveals differences in the distribution of the primary relaxation times, recalling the concept of Jonsher [50] via relations:

$$\frac{d\log_{10}\varepsilon''(f)}{d\log_{10}f} = m \quad \text{for } f < f_{peak} \quad \text{and} \quad \frac{d\log_{10}\varepsilon''(f)}{d\log_{10}f} = -n \quad \text{for } f > f_{peak} \tag{9}$$

where m and n denote coefficients describing the distribution of the relaxation time for the low- and the high-frequency parts of the loss curve, respectively.

The distribution of relaxation times is strongly non-Debye. For the spectrum under the weak electric field $m \sim 1/2$ (the low-frequency part) and $n \sim 1/2$ (high-frequency part). The latter was previously indicated by Olsen and Dyre [51] and later also in refs. [52, 53] as a

Preprints (www.preprints.org) | NOT PEER-REVIEWED | Posted: 6 July 2021 doi:10.20944/preprints202107.0155.v1

possibly universal value for the $T \to T_g$ path. However, under the strong electric field, the high-frequency part of the primary relaxation loss curve broadens: $n\left(T \to T_g\right) \sim 1/3$.

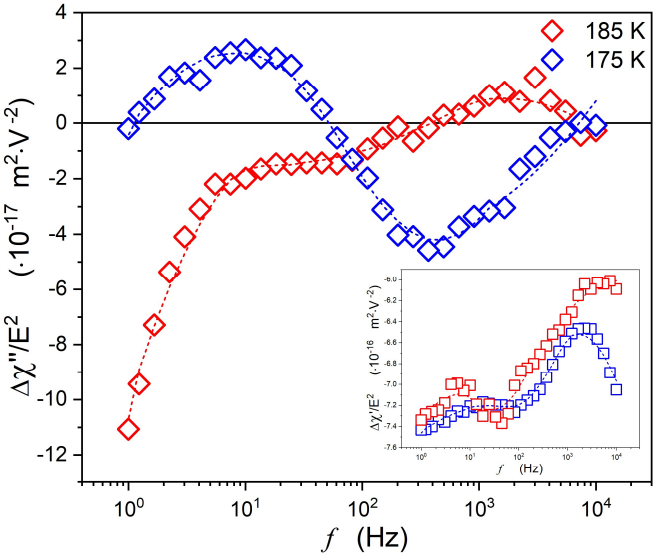

Figure 4 Examples of nonlinear dielectric spectra for the imaginary part of dielectric susceptibility $\Delta\varepsilon'' \equiv \Delta\chi'' = \chi''_{hi} - \chi''_{lo}$, where $\chi = \varepsilon - 1$, in the supercooled domain near the glass transition for $T < T_B^*$ and $T > T_B^*$.

The example of the distribution of relaxation processes related to the increment induced by the strong electric field is shown in Figure 4. It is noteworthy that its form is different from the one reported for the supercooled low-molecular-weight liquid and resembles the one observed in glass-forming orientationally disordered crystals. This scan suggests that for the ultraviscous supercooled squalene the detected processes are mainly associated with the orientation of permanent dipole moment. The hindering of translational molecular motions may be associated with the elongated and complex molecular structure of squalene.

Preprints (www.preprints.org) | NOT PEER-REVIEWED | Posted: 6 July 2021 doi:10.20944/preprints202107.0155.v1

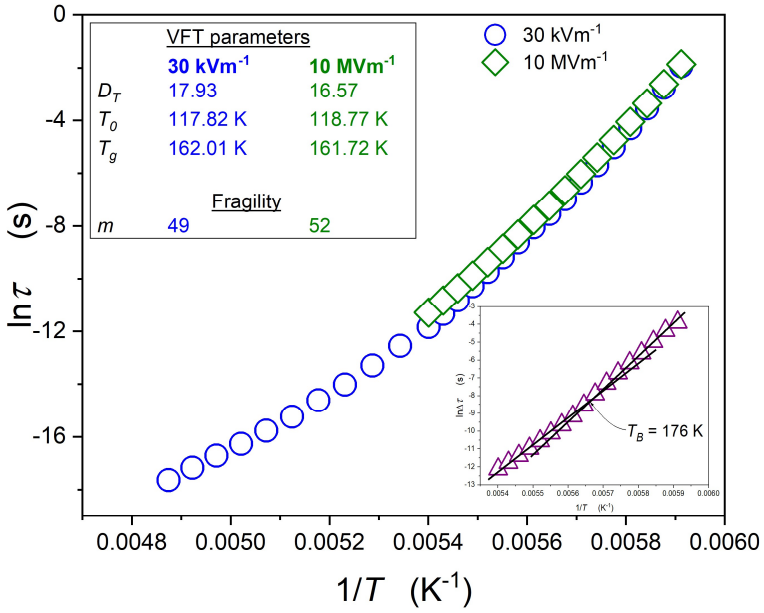

Figure 5 Relaxation map for supercooled squalene in weak (30 kV/m) and strong (10 MV/m) electric field. The insert presents a difference between relaxation times $\Delta\tau = \tau^{hi} - \tau^{lo}$ with visible singularity $T_B = T_{max} = 176$ K (comp. with Figure 2).

Figure 5 enables the comparison of the temperature evolution of the primary relaxation times under weak and strong electric field. The inset presents the difference in the relaxation time under weak and strong electric fields.

The reliable portrayal of previtreous changes of the primary relaxation times remains a non-conclusive challenge despite decades of studies. The set of competing for scaling relations yielding comparable, within the limit of the experimental error, fitting quality have been developed. In fact, such experimental evidence creates an essential problem for any theoretical modelling. In the opinion of the authors, the non-conclusiveness of studies can be explained by the fact that the analysis is carried out above T_g, ie., well beyond a hypothetical singular temperature included in experimental scaling relation. The experimental error strengthens the problem. A possible solution for the problem can offer the distortions-sensitive analysis. We propose to apply to experimental data presented in Figure 5 the analysis exploring the apparent activation index, based on the following transformation [54-56]:

$$\tau(T) \quad \Rightarrow \quad I_{DO}(T) = -\frac{d\ln E_a(T)}{d\ln T} = \frac{dE_a(T)/E_a(T)}{dT/T} \tag{10}$$

The application of Eq. (10) f requires a priori knowledge of the apparent activation energy. In refs. [54, 55] it was calculated in the previtreous domain using SA Eq. (1), namely $E_a(T) = RT\ln(\tau/\tau_0)$, assuming the universal and constant value of the pre-factor $\tau_0 = 10^{-14}\,s$. However, such a way of analysis can yield strongly biased values. To avoid such an impact a new way of determining $E_a(T)$ was proposed in refs. [56-58]. For a given set of $\tau(T)$ experimental data a numerical solution was used. Basing on the differential equation derived from the SA Eq. (1):

$$\frac{H_a(T)}{RT} = \frac{dE_a(T)}{d(1/T)} + E_a(T) \tag{11}$$

where $H_a(T) = d\ln\tau(T)/d(1/T)$ denotes the apparent activation enthalpy.

Preprints (www.preprints.org) | NOT PEER-REVIEWED | Posted: 6 July 2021 doi:10.20944/preprints202107.0155.v1

The analysis is supplemented by the final numerical filtering cleaning. On the basis of these results, the activation energy index in the ultraviscous domain has been analysed. It was empirically found that in each case, the reciprocal of the index follows the simple linear dependence [56-58]: $\frac{1}{I_{DO}(T)} = aT + b$. It is worth stressing that such a behaviour agrees well with the indexes derived for the basic model-equation, namely [56]: (i) $1/I_{DO} = (1/T_0)T - 1$ for the VFT Eq. (2), (ii) $1/I_{DO} = (1/C)T$ for the WM (MYEGA) Eq. (3) and (iii) $1/I_{DO} = (1/\phi)T - (T_C/\phi)$ for the critical-like Eq. (4). It was empirically proved that for systems studied in refs. [56] the coefficient $n = -1/b$ is located between 0.2 and 1.6. The highest value is for glass formers showing the uniaxial symmetry, such as liquid crystalline, where the critical-like behaviour is preferred (Eq. (5)). Values $n \sim 0.2$ were noted for orientationally disordered crystals. Values $n \approx 1$ can be linked to the VFT Eq. (2): in ref. [56] it was called the 'no-symmetry case'.

Figure 6 shows the behaviour of the apparent activation index (A) determined for the ultraviscous supercooled squalene as well as the configurational entropy S_C (B) given by

$$S_C(T) = S_0\left(1 - \left(\frac{b}{a}\right)\frac{1}{T}\right)^{-1/b} = S_0\left(1 - \frac{T_N}{T}\right)^n \qquad (12)$$

where $T_N = |b/a|$ is the singular temperature denoted the Kauzmann temperature $T_N = T_K$ and $n = -1/b$ describes power exponent. Notably, for the VFT relation the $n = 1$, $T_N = T_K = T_0$.

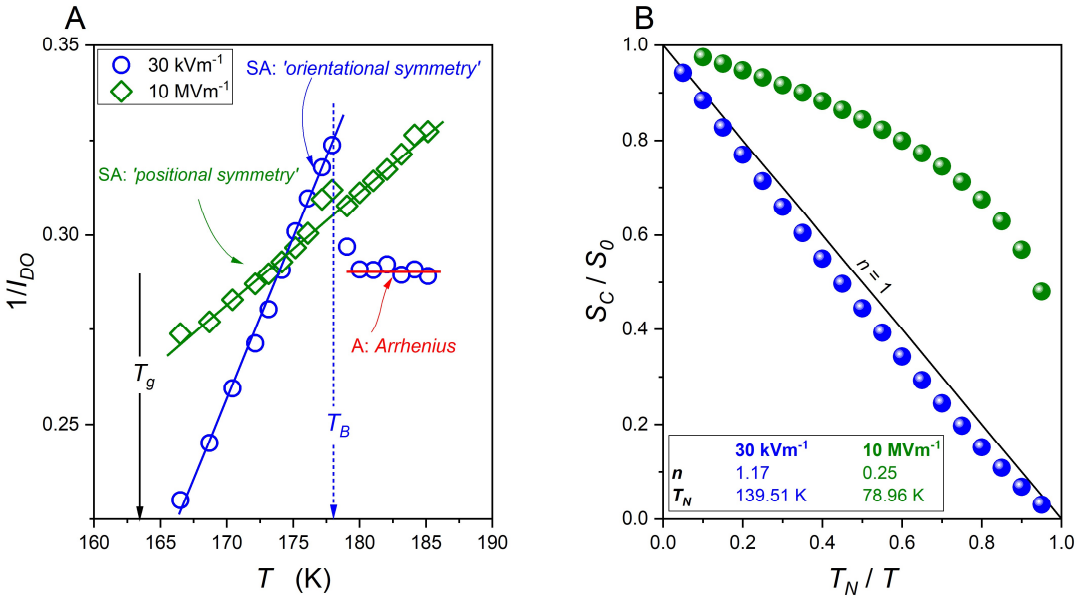

Figure 6 (A) Changes of the reciprocal of the apparent activation index I_{DO} (Eq. (10)) for supercooled squalene, based on experimental data given in Fig. 5. **(B)** Configurational entropy S_C for squalene under weak (blue) and strong (green) electric field calculated from Eq. (12). Parameters with $n = 1.17$, $T_N = 139.51$ K and $n = 0.25$, $T_N = 78.96$ K for weak and strong electric field, respectively, were obtained using Eq. (12).

There is an explicit straight-line behaviour of $1/I_{DO}(T)$ the crossover $1/I_{DO}^{wEF} > 1/I_{DO}^{sEF} \rightarrow 1/I_{DO}^{wEF} < 1/I_{DO}^{sEF}$ on cooling towards the glass temperature. The values of the coefficient n show that the dynamics of squalene can be well described by the critical-like Eq. (4), The application of the strong electric field shifts dynamics to the VFT Eq. (3) patterns.

Preprints (www.preprints.org) | NOT PEER-REVIEWED | Posted: 6 July 2021 doi:10.20944/preprints202107.0155.v1

Worth indicating is the link between the activation index and the apparent fragility $m(T)=C(1+I_{DO}(T))$, where $C=2-log_{10}\tau_0$ [56-58]. This suggests similar temperature dependences for $I_{DO}(T)$ and $m(T)$. The hypothetically universal linear changes of $1/m(T)$ were first shown in ref. [48] for a variety of glass formers. Notably, the same temperature dependence can be expected for $1/m(T)$, $1/H_a(T)$ and $1/(d\,ln\,\tau(T)/d(1/T))$ vs. T plots [48].

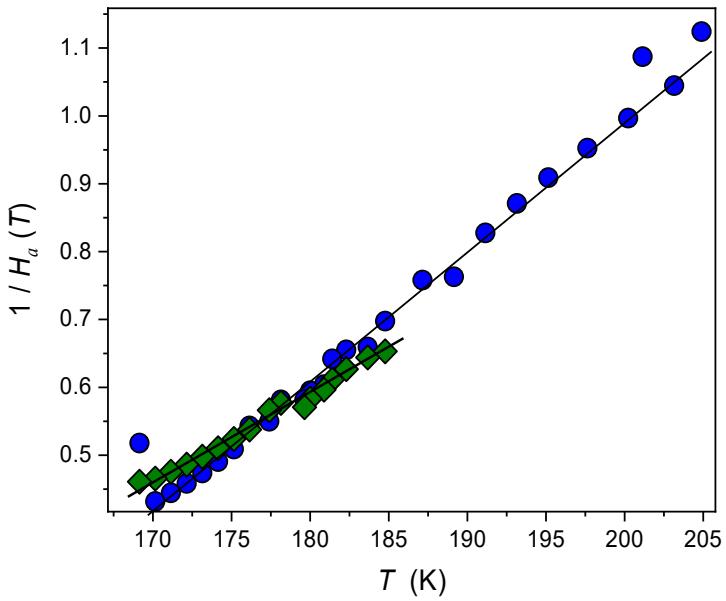

Figure 7 Linear temperature changes of the reciprocal of the apparent activation enthalpy in supercooled squalene under weak and strong electric field on approaching the glass temperature. Note the relation to the apparent fragility: $1/H_a(T)\propto 1/m(T)$.

Such a behaviour is shown in Figure 7. Two linear dependences intersecting at $T_{max}\approx 176K$ can be seen. It is worth noting that for $T>T_{max}$ the fragility index of the ultraviscous squalene is higher under weak electric field than for the same system when the strong electric field is applied. For $T<T_{max}$ the same situation occurs.

Nonlinear dielectric studies originate from nonlinear dielectric effect investigations exhibiting changes of dielectric constant under strong electric field. A century ago, Herweg [59] performed the first-ever NDE test of diethyl ether, obtaining $\frac{\Delta\chi^E}{E^2}\sim 10^{-18}m^2V^{-2}$. Debye explained this phenomenon as the consequence of the orientation of the almost non-interacting permanent dipole moments incorporating and developing the dielectric Langevin series [60]. Two decades later, Piekara discovered a strong, positive NDE in nitrobenzene due to the dipole-dipole coupling [61]. Next, he found an anomalous positive increase of NDE on approaching the critical consolute point in binary mixtures of limited miscibility [62]. Not until 1999 the latter phenomenon, as well as the similar effect in the isotropic liquid phase of rod-like liquid crystals (LC), was explained as the consequence of the interactions within the pretransitional fluctuations by using the model-relation [63, 64]:

$$\frac{\Delta\chi^E}{E^2}=\frac{\Delta\varepsilon^E}{E^2}\propto\langle\Delta M^2\rangle_V\chi_T \qquad (13)$$

Preprints (www.preprints.org) | NOT PEER-REVIEWED | Posted: 6 July 2021 doi:10.20944/preprints202107.0155.v1

where $\langle \Delta M^2 \rangle_V$ is for the local fluctuations of the mean square of the order parameter and χ_T denotes order parameter related susceptibility (compressibility).

For the isotropic phase of LC materials $\langle \Delta M^2 \rangle_V = const$ and $\chi_T(T) = \chi_0 / (T - T^*)$, where T^* denotes the extrapolated temperature of a hypothetical continuous phase transition. Consequently, for rod-like LC materials $\Delta\varepsilon^E / E^2 \propto 1/(T - T^*)$ [63, 55-67].

The pretransitional effect has been discovered for the isotropic liquid – plastic crystal phase transition in cyclooctanol. Its form can be well portrayed by the following relation [41]:

$$\frac{\Delta\chi^E}{E^2}(T) = e^* + a_E(T - T^*) + A_E(T - T^*)^{\phi=0.5} \quad (14)$$

It was indicated that the above relation could also result from Eq. (13) on assuming that for ODIC-forming materials, hardly compressible semi-solid fluctuations in the liquid phase occur. Hence $\chi_T \approx const$. However, the dielectric constant of pre-ODIC fluctuations strongly differs from the dielectric constant of the isotropic liquid surroundings, particularly under the strong electric field resulting from the free orientation of the permanent dipole moments. Consequently, the temperature dependence of the order parameter plays the key role in Eq. (13): $\langle \Delta M^2 \rangle_V \propto (T - T^*)^{2\beta}$, where β is the order parameter exponent. Assuming for the latter the classical tricritical value $\beta = 1/4$ [39] and the linear temperature dependence for the non-critical background, one can obtain Eq. (14).

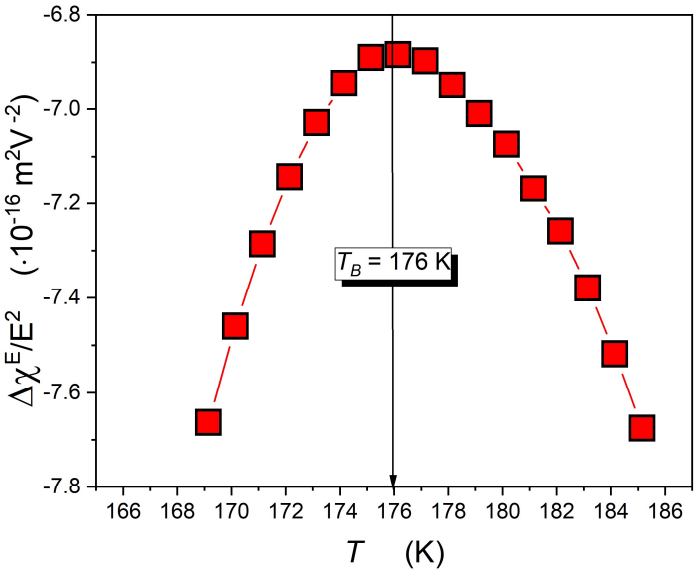

Figure 8 Nonlinear dielectric effect (NDE) on approaching the glass temperature in ultraviscous, supercooled squalene. The curve portraying experimental data is related to Eq. (14).

Figure 8 shows the temperature changes of NDE exhibiting changes that can be well portrayed by Eq. (14). It is worth noting that the characteristic maximum of the relation $\Delta\chi^E/E^2(T)$ occurs for the same temperature as it results in Figs. 5 and 6. From Eq. (14) the region $T_g < T < T_{max}$ is dominated by pretransitional previtreous fluctuations.

IV. CONCLUSIONS

This paper shows evidence for the long-range pretransitional/previtreous behaviour of two static properties: dielectric constant and its strong electric field related counterpart, the nonlinear dielectric effect. Notable is the possibility of their functional characterizations by Eq.

(8), with the 'Mossotti Catastrophe' form, and Eq. (12) resembling the formula developed for critical liquids. The analysis of dynamic properties based on the activation energy index excluded the VFT relation (associated with the coefficient $n = 1$) as a validated tool for portraying the evolution of the primary relaxation time in squalene, both under weak and strong electric field. Such results question the commonly applied 'Stickel operator' routine, used as the tool for determining the dynamic crossover between the high- and low- temperatures dynamic domains in the supercooled state. It is worth stressing that the strong electric field radically affects the distribution of relaxation times, the form of the evolution of the primary relaxation time, and the fragility metric.

V. ACKNOWLEDGMENTS

This research was carried out due to the support of the National Centre for Science (Poland) projects: OPUS ref. 2016/21/B/ST3/02203, head Aleksandra Drozd-Rzoska and ETIUDA ref. 2019/32/T/ST3/00621 leaded by Szymon Starzonek.

VI. AUTHOR'S CONTRIBUTION

All authors contributed equally to this work

VII. DATA AVABILITY

The data that supports the findings of this study are available within the paper.

VIII. REFERENCES

1. Kim, S. K., Karadeniz, F. (2012). Biological importance and applications of squalene and squalane. In *Advances in food and nutrition research* (Vol. 65, pp. 223-233). Academic Press.
2. Rao, C. V., Newmark, H. L., & Reddy, B. S. (1998). Chemopreventive effect of squalene on colon cancer. *Carcinogenesis*, *19*(2), 287-290.
3. Passi, S., De Pità, O., Puddu, P., Littarru, G. P. (2002). Lipophilic antioxidants in human sebum and aging. *Free radical research*, *36*(4), 471-477.
4. Huang, Z. R., Lin, Y. K., Fang, J. Y. (2009). Biological and pharmacological activities of squalene and related compounds: potential uses in cosmetic dermatology. *Molecules*, *14*(1), 540-554.
5. Camera, E., Ottaviani, M., Picardo, M. (2015). Squalene chemistry and biology. In *Lipids and Skin Health* (pp. 185-198). Springer, Cham. Papas A. (ed.) Lipids and Skin Healths (Springer, Berlin, 2014).
6. Narayan Bhilwade, H., Tatewaki, N., Nishida, H., Konishi, T. (2010). Squalene as novel food factor. *Current Pharmaceutical Biotechnology*, *11*(8), 875-880.
7. Özge Seçmeler, Charis M. Galanakis (eds), Innovations in Traditional Foods (Woodhead Publ. - Elsevier, Amstertdam, 2019).
8. Kowert, B. A., Watson, M. B. (2011). Diffusion of organic solutes in squalane. *The Journal of Physical Chemistry B*, *115*(32), 9687-9694.
9. Ruiz-Mercado, G., Cabezas, H., Sustainability in the Design, Synthesis and Analysis of Chemical Engineering Process (Elsevier, Amsterdam.2016).
10. Gohil, N., Bhattacharjee, G., Khambhati, K., Braddick, D., Singh, V. (2019). Corrigendum: Engineering Strategies in Microorganisms for the Enhanced Production of Squalene: Advances, Challenges and Opportunities. *Frontiers in bioengineering and biotechnology*, *7*.
11. Dean, J.A., Lange's Handbook of Chemistry (McGraw-Hill, NY, 1999)
12. Berthier, L., Ediger, M. Facets of glass physics. *Physics Today* 69, 40-44 (2016).

13. Lubchenko, V. (2017). Glass transition imminent, resistance is futile. *Proceedings of the National Academy of Sciences*, *114*(13), 3289-3291.
14. Ninarello, A., Berthier, L., Coslovich, D. (2017). Models and algorithms for the next generation of glass transition studies. *Physical Review X*, *7*(2), 021039.
15. Kremer, F., Loidl, A. Scaling of Relaxation Processes (Springer, Berlin, 2018).
16. Angell, C. A. Strong and fragile liquids, in: *Relaxations in Complex Systems*, eds. Ngai, K. L. and Wright, G. B. (National Technical Information Service, U.S. Dept. of Commerce, Springfield, 1985).
17. Böhmer, R., Ngai, K. L., Angell, C. A., Plazek, D. J. (1993). Nonexponential relaxations in strong and fragile glass formers. *The Journal of chemical physics*, *99*(5), 4201-4209.
18. Vogel, H. Das temperature-abhängigketsgesetz der viskosität von flüssigkeiten *Phys. Zeit.* 22, 645–646 (1921).
19. Fulcher, G. S. (1925). Analysis of recent measurements of the viscosity of glasses. *Journal of the American Ceramic Society*, *8*(6), 339-355.
20. Tammann, G. Glasses as supercooled liquids. *J. Soc. Glass Technol.* 9, 166–185 (1925).
21. Mauro, J. C., Yue, Y., Ellison, A. J., Gupta, P. K., Allan, D. C. (2009). Viscosity of glass-forming liquids. *Proceedings of the National Academy of Sciences*, *106*(47), 19780-19784.
22. Romanini, M., Martinez-Garcia, J. C., Tamarit, J. L., Rzoska, S. J., Barrio, M., Pardo, L. C., Drozd-Rzoska, A. (2009). Scaling the dynamics of orientationally disordered mixed crystals. *The Journal of chemical physics*, *131*(18), 184504.
23. Drozd-Rzoska, A., Rzoska, S. J., Pawlus, S., Martinez-Garcia, J. C., Tamarit, J. L. (2010). Evidence for critical-like behavior in ultraslowing glass-forming systems. *Physical Review E*, *82*(3), 031501.
24. Drozd-Rzoska, A., Rzoska, S. J., Pawlus, S., Tamarit, J. L. (2006). Dielectric relaxation in compressed glassy and orientationally disordered mixed crystals. *Physical Review B*, *74*(6), 064201.
25. Drozd-Rzoska, A. (2006). Heterogeneity-related dynamics in isotropic n-pentylcyanobiphenyl. *Physical Review E*, *73*(2), 022501.
26. Drozd-Rzoska, A. (2009). Glassy dynamics of liquid crystalline 4′-n-pentyl-4-cyanobiphenyl in the isotropic and supercooled nematic phases. *The Journal of chemical physics*, *130*(23), 234910.
27. Donth, E.J. The Glass Transition. Relaxation Dynamics in Liquids and Disordered Materials (Springer, Berlin, 2004).
28. Rzoska, S.J., Mazur, V., Drozd-Rzoska, A. (eds.), Metastable Systems under Pressure (Springer Verlag, Berlin, 2010).
29. Drozd-Rzoska, A., Rzoska, S. J., Ziolo, J., & Czuprynski, K. (1999). Nonlinear dielectric studies in supercooling 4-(2-methylbutyl)-4′-cyanobiphenyl (5* CB). *Journal of Physics: Condensed Matter*, *11*(43), L473.
30. Young-Gonzales, A. R., Adrjanowicz, K., Paluch, M., Richert, R. (2017). Nonlinear dielectric features of highly polar glass formers: Derivatives of propylene carbonate. *The Journal of chemical physics*, *147*(22), 224501.
31. Häberle, U., Diezemann, G. (2006). Kerr effect as a tool for the investigation of dynamic heterogeneities. *The Journal of chemical physics*, *124*(4), 044501.
32. Rzoska, S. J., Drozd-Rzoska, A. (2011). Dual field nonlinear dielectric spectroscopy in a glass forming EPON 828 epoxy resin. *Journal of Physics: Condensed Matter*, *24*(3), 035101.

33. Gadige, P., Albert, S., Michl, M., Bauer, T., Lunkenheimer, P., Loidl, A., Ladieu, F. (2017). Unifying different interpretations of the nonlinear response in glass-forming liquids. *Physical Review E*, *96*(3), 032611.
34. Albert, S., Bauer, T., Michl, M., Biroli, G., Bouchaud, J. P., Loidl, A., Ladieu, F. (2016). Fifth-order susceptibility unveils growth of thermodynamic amorphous order in glass-formers. *Science*, *352*(6291), 1308-1311.
35. Michl, M., Bauer, T., Lunkenheimer, P., Loidl, A. (2016). Nonlinear dielectric spectroscopy in a fragile plastic crystal. *The Journal of chemical physics*, *144*(11), 114506.
36. Richert, R. (2018). Perspective: Nonlinear approaches to structure and dynamics of soft materials. *The Journal of chemical physics*, *149*(24), 240901.
37. Richert, R. (Ed.) Nonlinear Dielectric Spectroscopy (Springer, Berlin, 2018).
38. Stanley, H.E. Introduction to Phase Transition and Critical Phenomena (Oxford Univ. Press., Oxford, 1971 and 1987).
39. Anisimov, M.A. Critical Phenomena in Liquids and Liquid Crystals (Gordon and Breach, Reading, 1994).
40. Gitterman, M. Chemistry versus Physics. Chemical Reactions Near Critical Points (World Sci. Publ., London, 2010).
41. Drozd-Rzoska, A.; Starzonek, S.; Rzoska, S.J.; Łoś, J.; Kutnjak, Z.; Kralj, S. Pretransitional Effects of the Isotropic Liquid–Plastic Crystal Transition. *Molecules* 2021, *26*, 429
42. https://www.novocontrol.de/php/a_harm.php
43. Chelkowski, A. Dielectric Physics (PWN-Elsevier. Warsaw. 1990).
44. S. J. Rzoska and V. Mazur (eds.), Soft Matter under Exogenic Impacts" NATO Sci. Series II, vol. 242 (Springer, Berlin, 2007).
45. Rzoska, S., Zioło, J., Drozd-Rzoska, A., Tamarit, J. L., Veglio, N. (2008). New evidence for a liquid–liquid transition in a one-component liquid. *Journal of Physics: Condensed Matter*, *20*(24), 244124.
46. Stevenson, J. D., Wolynes, P. G. (2005). Thermodynamic− Kinetic Correlations in Supercooled Liquids: A Critical Survey of Experimental Data and Predictions of the Random First-Order Transition Theory of Glasses. *The Journal of Physical Chemistry B*, *109*(31), 15093-15097.
47. Stickel, F., Fischer, E. W., Richert, R. (1996). Dynamics of glass-forming liquids. II. Detailed comparison of dielectric relaxation, dc-conductivity, and viscosity data. *The Journal of chemical physics*, *104*(5), 2043-2055.
48. Drozd-Rzoska, A. (2019). Universal behavior of the apparent fragility in ultraslow glass forming systems. *Scientific reports*, *9*(1), 1-9.
49. Drozd-Rzoska, A. (2019). Pressure-related universal previtreous behavior of the structural relaxation time and apparent fragility. *Frontiers in Materials*, *6*, 103.
50. Jonscher, A. K. (1977). The 'universal' dielectric response. *Nature*, *267*(5613), 673-679.
51. Nielsen, A. I., Christensen, T., Jakobsen, B., Niss, K., Olsen, N. B., Richert, R., Dyre, J. C. (2009). Prevalence of approximate t relaxation for the dielectric α process in viscous organic liquids. *The Journal of chemical physics*, *130*(15), 154508.
52. Nielsen, A. I., Pawlus, S., Paluch, M., Dyre, J. C. (2008). Pressure dependence of the dielectric loss minimum slope for ten molecular liquids. *Philosophical Magazine*, *88*(33-35), 4101-4108.
53. Martinez-Garcia, J. C., Tamarit, J. L., Rzoska, S. J. (2011). Prevalence for the universal distribution of relaxation times near the glass transitions in experimental

model systems: Rodlike liquid crystals and orientationally disordered crystals. *The Journal of chemical physics*, *134*(14), 144505.
54. Dyre, J. C., Olsen, N. B. (2004). Landscape equivalent of the shoving model. *Physical Review E*, *69*(4), 042501.
55. Hecksher, T., Nielsen, A. I., Olsen, N. B., Dyre, J. C. (2008). Little evidence for dynamic divergences in ultraviscous molecular liquids. *Nature Physics*, *4*(9), 737-741.
56. Martinez-Garcia, J. C., Rzoska, S. J., Drozd-Rzoska, A., Martinez-Garcia, J. (2013). A universal description of ultraslow glass dynamics. *Nature communications*, *4*(1), 1-9.
57. Martinez-Garcia, J. C., Rzoska, S. J., Drzozd-Rzoska, A., Martinez-Garcia, J., Mauro, J. C. (2014). Divergent dynamics and the Kauzmann temperature in glass forming systems. *Scientific reports*, *4*, 5160.
58. Martinez-Garcia, J. C., Rzoska, S. J., Drozd-Rzoska, A., Starzonek, S., Mauro, J. C. (2015). Fragility and basic process energies in vitrifying systems. *Scientific reports*, *5*, 8314.
59. Herweg, J. (1920). Die elektrischen Dipole in flüssigen Dielektricis. *Zeitschrift für Physik*, *3*(1), 36-47.
60. Debye, P. (1935). Die elektrischen Dipole in flüssigen Dielektricis. *Phys. Z*, *36*, 193.
61. Piekara, A., Piekara, B. (1936). Saturation électrique dans les liquides purs et leurs mélanges. *CR Acad. Sci*, *203*, 852.
62. Piekara, A. (1936). Saturation electrique et point critique de dissolution (presente par Aime Cotton). *CR Acad Sci. Paris*, *203*, 1058-1059.
63. Rzoska, S. J. (1993). Kerr effect and the nonlinear dielectric effect on approaching the critical consolute point. *Physical Review E*, *48*(2), 1136.
64. Drozd-Rzoska, A., Rzoska, S. J., Martinez-Garcia, J. C. (2014). Nonlinear dielectric effect in supercritical diethyl ether. *The Journal of chemical physics*, *141*(9), 094907.
65. Drozd-Rzoska, A., Rzoska, S. J., Zioło, J. (1996). Mean-field behaviour of the low frequency non-linear dielectric effect in the isotropic phase of nematic and smectic n-alkylcyanobiphenyls. *Liquid crystals*, *21*(2), 273-277.
66. Drozd-Rzoska, A., Rzoska, S. J., Zioło, J. (1997). High-pressure studies of the low-frequency nonlinear dielectric effect in the isotropic phaseof octyl-and dodecylcyanobiphenyls. *Physical Review E*, *55*(3), 2888.
67. Drozd-Rzoska, A., Rzoska, S. J., Czupryński, K. (2000). Phase transitions from the isotropic liquid to liquid crystalline mesophases studied by linear and nonlinear static dielectric permittivity. *Physical Review E*, *61*(5), 5355.